

Boise State University

ScholarWorks

Materials Science and Engineering Faculty
Publications and Presentations

Micron School for Materials Science and
Engineering

1-21-2023

Probing DNA Structural Heterogeneity by Identifying Conformational Subensembles of a Bicovalently Bound Cyanine Dye

Matthew S. Barclay
Boise State University

Azhad U. Chowdhury
Boise State University

Austin Biaggne
Boise State University

Jonathan S. Huff
Boise State University

Nicholas D. Wright
Boise State University

See next page for additional authors

Authors

Matthew S. Barclay, Azhad U. Chowdhury, Austin Biaggne, Jonathan S. Huff, Nicholas D. Wright, Paul H. Davis, Lan Li, William B. Knowlton, Bernard Yurke, Ryan D. Pensack, and Daniel B. Turner

Probing DNA structural heterogeneity by identifying conformational subensembles of a bicovalently bound cyanine dye

Cite as: *J. Chem. Phys.* **158**, 035101 (2023); doi: [10.1063/5.0131795](https://doi.org/10.1063/5.0131795)

Submitted: 24 October 2022 • Accepted: 29 December 2022 •

Published Online: 18 January 2023














View Online



Export Citation



CrossMark

Matthew S. Barclay,¹  Azhad U. Chowdhury,¹  Austin Biagne,¹  Jonathan S. Huff,¹ 
Nicholas D. Wright,¹  Paul H. Davis,^{1,2}  Lan Li,^{1,2}  William B. Knowlton,^{1,3}  Bernard Yurke,^{1,3} 
Ryan D. Pensack,^{1,a)}  and Daniel B. Turner^{1,b)} 

AFFILIATIONS

¹ Micron School for Materials Science and Engineering, Boise State University, Boise, Idaho 83725, USA

² Center for Advanced Energy Studies, Idaho Falls, Idaho 83401, USA

³ Department of Electrical and Computer Engineering, Boise State University, Boise, Idaho 83725, USA

Note: This paper is part of the JCP Special Topic on Celebrating 25 Years of Two-dimensional Infrared (2D IR) Spectroscopy.

^{a)} **Electronic mail:** ryanpensack@boisestate.edu

^{b)} **Author to whom correspondence should be addressed:** danielturner926@boisestate.edu

ABSTRACT

DNA is a re-configurable, biological information-storage unit, and much remains to be learned about its heterogeneous structural dynamics. For example, while it is known that molecular dyes templated onto DNA exhibit increased photostability, the mechanism by which the structural dynamics of DNA affect the dye photophysics remains unknown. Here, we use femtosecond, two-dimensional electronic spectroscopy measurements of a cyanine dye, Cy5, to probe local conformations in samples of single-stranded DNA (ssDNA–Cy5), double-stranded DNA (dsDNA–Cy5), and Holliday junction DNA (HJ–DNA–Cy5). A line shape analysis of the 2D spectra reveals a strong excitation–emission correlation present in only the dsDNA–Cy5 complex, which is a signature of inhomogeneous broadening. Molecular dynamics simulations support the conclusion that this inhomogeneous broadening arises from a nearly degenerate conformer found only in the dsDNA–Cy5 complex. These insights will support future studies on DNA’s structural heterogeneity.

© 2023 Author(s). All article content, except where otherwise noted, is licensed under a Creative Commons Attribution (CC BY) license (<http://creativecommons.org/licenses/by/4.0/>). <https://doi.org/10.1063/5.0131795>

I. INTRODUCTION

For functions essential to life, DNA must be able to both store and translate genetic information. Therefore, the structure of DNA under physiological conditions must have the right balance of flexibility and rigidity so that these biological macromolecules are amenable to large conformational changes. For example, thermally induced conformational fluctuations that occur on the timescale of microseconds to seconds are referred to as “breathing,” which originate from the interplay of hydrogen bonding and other intermolecular forces operating simultaneously.¹ The conformational variability and complementarity of the nucleobase pairing is not only important for fundamental studies, but it has spawned the fields of

structural² and dynamic³ DNA nanotechnology. The programmability afforded by the Watson–Crick base pairing has proved to be a powerful means with which to organize matter on the nanoscale, as manifested by the variety of DNA nanostructures that have been fabricated.^{4–7} The flexibility of DNA has enabled the animation of matter on the nanoscale, as manifested by the variety of nanomachines and devices driven by hybridization and strand–displacement reactions that have been constructed.^{8–11} While the conformational variability of DNA is advantageous in the construction of dynamic DNA structures, it limits the rigidity of DNA-based nanostructures. This has led to an interest in developing the means to engineer the rigidity of nucleic acid-based structures^{12–15} and the dynamic stability of DNA-nanostructures.¹⁶

The mechanisms that give rise to the conformational changes of DNA have been studied using a multitude of techniques, many of which are optical microscopy and spectroscopy methods that probe dyes that are attached to DNA. Indeed, dyes that are covalently bound to a DNA or another biological macromolecule are often used as probes of the local changes, in conformation with single-molecule spectroscopy studies.^{17–20} Due to their convenient optical and chemical properties, commercially available cyanine dyes, such as Cy5, are often used in these types of optical studies.²¹ In addition to studies in which a dye is used to probe the DNA structure, studies in which researchers use DNA nanostructures as a scaffold or template to form and study molecular aggregates are also common.^{22–26}

Coherent multidimensional optical spectroscopy is a technique that combines the signal specificity of multidimensional nuclear magnetic resonance spectroscopy with the femtosecond time resolution of transient absorption spectroscopy.^{27–30} This family of spectroscopy methods—now approaching its 25th anniversary as celebrated in this special issue—has also been applied to learn more about DNA structures and structural changes in a few instances, including 2D infrared³¹ and 2D fluorescence spectroscopy studies.^{32,33} Two-dimensional electronic spectroscopy (2D ES)—which is most often performed with a sequence of femtosecond laser pulses at visible wavelengths—has yet to be applied to study structural changes of DNA. Indeed, this four-wave mixing method has most notably been used to study the mechanisms of electronic energy transfer in photosynthetic systems.^{34–38} Yet, the rephasing property of 2D ES enables the method to overcome some of the ensemble averaging that leads to broad line shapes in conventional spectroscopy techniques, and this way, it can provide insights into sub-ensembles similar to single-molecule methods. This makes the technique a viable method to identify and analyze heterogeneous distributions of DNA structures in ensemble measurements.

In this contribution, we use 2D ES measurements—supported by a theoretical model and computational results—to study four Cy5 monomer samples, three of which are attached to various forms of DNA. The 2D ES of the free Cy5 dye, the single-stranded DNA attached to Cy5 (ssDNA–Cy5), and the Cy5 attached in a four-armed DNA Holliday junction (HJ–DNA–Cy5) sample—all show very little correlation between the excitation and emission frequencies. This suggests that the solutions either lack heterogeneity or the dye is free to fluctuate among all allowed configurations quickly enough to explore all energetically distinct environments within the duration of the measurement. In contrast, the 2D spectra of the sample in which Cy5 is attached to double-stranded DNA (dsDNA–Cy5) show strong correlation between excitation and emission frequencies, which persists for the duration of the measurement. This correlation arises from an inhomogeneous broadening mechanism in the dsDNA–Cy5 sample that restricts the Cy5 from exploring all possible allowed energetically distinct conformations.

II. THEORETICAL

To simulate the effect of inhomogeneous broadening in 2D spectra arising from multiple DNA–Cy5 configurations, here, we present a model that uses the response-function formalism applied to a three-level electronic system model including static inhomogeneous broadening.³⁹ We include states $|g\rangle$, $|e\rangle$, and $|f\rangle$, having

energies ϵ_g , ϵ_e , and ϵ_f , respectively. Following the crude adiabatic approximation,⁴⁰ the molecular Hamiltonian is given by

$$\hat{H} = \sum_{i \in \{g,e,f\}} \epsilon_i |i\rangle \langle i|. \quad (1)$$

There are two optically allowed transitions— $|g\rangle \rightarrow |e\rangle$ and $|e\rangle \rightarrow |f\rangle$. The main resonance has a transition frequency ω_{eg} , with transition dipole μ_{eg} , and the excited-state absorption pathways have a frequency ω_{fe} , with transition dipole μ_{fe} . Under the Condon approximation, the transition-dipole operator is given by

$$\hat{V} = \mu_{eg} |e\rangle \langle g| + \mu_{fe} |f\rangle \langle e| + H.c., \quad (2)$$

where $H.c.$ refers to the Hermitian conjugate. A 2D spectrum arises from a two-dimensional Fourier transformation of the third-order nonlinear signal

$$S_{2D}(\omega_1, \tau_2, \omega_3) = \mathcal{F}_{\tau_1, \tau_3} \left[S^{(3)}(\tau_1, \tau_2, \tau_3) \right], \quad (3)$$

where the third-order nonlinear signal is a function of the time intervals τ_1 , τ_2 , and τ_3 among the laser pulses, which we assume to be impulsive under the rotating wave approximation. The signal can then be written as a sum of six response functions

$$S^{(3)}(\tau_1, \tau_2, \tau_3) = \left(\frac{i}{\hbar} \right)^3 \theta(\tau_1) \theta(\tau_2) \theta(\tau_3) \sum_{j=1}^6 \left[R_j(\tau_1, \tau_2, \tau_3) - R_j^*(\tau_1, \tau_2, \tau_3) \right]. \quad (4)$$

The response functions based on a Bloch model are given by

$$\begin{aligned} R_1^{(3)}(\tau_1, \tau_2, \tau_3) &= R_4^{(3)}(\tau_1, \tau_2, \tau_3) \\ &= |\mu_{eg}|^4 \int d\Gamma W(\Gamma) e^{-i\omega_{eg}(\Gamma)(\tau_1+\tau_3)} \\ &\quad \times e^{-\gamma_{eg}(\tau_1+\tau_3)} e^{-\Gamma_p \tau_2}, \end{aligned} \quad (5a)$$

$$\begin{aligned} R_2^{(3)}(\tau_1, \tau_2, \tau_3) &= R_3^{(3)}(\tau_1, \tau_2, \tau_3) \\ &= |\mu_{eg}|^4 \int d\Gamma W(\Gamma) e^{+i\omega_{eg}(\Gamma)(\tau_1-\tau_3)} \\ &\quad \times e^{-\gamma_{eg}(\tau_1+\tau_3)} e^{-\Gamma_p \tau_2}, \end{aligned} \quad (5b)$$

$$\begin{aligned} R_5^{(3)}(\tau_1, \tau_2, \tau_3) &= -|\mu_{eg}|^2 |\mu_{fe}|^2 \int d\Gamma W(\Gamma) e^{+i\omega_{eg}(\Gamma)\tau_1} \\ &\quad \times e^{-i\omega_{fe}(\Gamma)\tau_3} e^{-\gamma_{eg}\tau_1} e^{-\gamma_{fe}\tau_3} e^{-\Gamma_p \tau_2}, \end{aligned} \quad (5c)$$

$$\begin{aligned} R_6^{(3)}(\tau_1, \tau_2, \tau_3) &= -|\mu_{eg}|^2 |\mu_{fe}|^2 \int d\Gamma W(\Gamma) e^{-i\omega_{eg}(\Gamma)\tau_1} \\ &\quad \times e^{-i\omega_{fe}(\Gamma)\tau_3} e^{-\gamma_{eg}\tau_1} e^{-\gamma_{fe}\tau_3} e^{-\Gamma_p \tau_2}, \end{aligned} \quad (5d)$$

where γ_{eg} and γ_{fe} are phenomenological dephasing parameters, Γ_p accounts for excited-state population relaxation, and the integral over Γ accounts for static inhomogeneous broadening of the transition frequencies.³⁹ Response functions $R_{\{2,3,5\}}^{(3)}$ are the rephasing pathways, while response functions $R_{\{1,4,6\}}^{(3)}$ are nonrephasing

pathways. Response functions $R_{\{5,6\}}^{(3)}$ account for the excited-state absorption components of the signal.

We, next, explicitly account for the static inhomogeneous broadening by taking the difference between the fundamental and excited-state absorption frequencies to be a constant, $\omega_{fe}(\Gamma) - \omega_{eg}(\Gamma) = \Delta$, the fundamental transition frequency to be given by a constant plus the fluctuation, $\omega_{eg}(\Gamma) = \omega_{eg} + \Gamma$, and the distribution to be Gaussian, $W(\Gamma) = \frac{1}{\sigma\sqrt{2\pi}} e^{-\Gamma^2/(2\sigma^2)}$, where σ is the standard deviation.³⁹ These substitutions yield

$$\int_{-\infty}^{+\infty} d\Gamma W(\Gamma) e^{+i\omega_{eg}(\Gamma)t} = e^{+i\omega_{eg}t} e^{-t^2\sigma^2/2}, \quad (6)$$

where t serves as a generic time argument. Using this result, the response functions become

$$\begin{aligned} R_1^{(3)}(\tau_1, \tau_2, \tau_3) &= R_4^{(3)}(\tau_1, \tau_2, \tau_3) \\ &= |\mu_{eg}|^4 e^{-i\omega_{eg}(\tau_1+\tau_3) - (\tau_1+\tau_3)^2\sigma^2/2} e^{-\gamma(\tau_1+\tau_3)}, \end{aligned} \quad (7a)$$

$$\begin{aligned} R_2^{(3)}(\tau_1, \tau_2, \tau_3) &= R_3^{(3)}(\tau_1, \tau_2, \tau_3) \\ &= |\mu_{eg}|^4 e^{+i\omega_{eg}(\tau_1-\tau_3) - (\tau_1-\tau_3)^2\sigma^2/2} e^{-\gamma(\tau_1+\tau_3)}, \end{aligned} \quad (7b)$$

$$\begin{aligned} R_5^{(3)}(\tau_1, \tau_2, \tau_3) &= -|\mu_{eg}|^2 |\mu_{fe}|^2 e^{-i\Delta\tau_3} e^{+i\omega_{eg}(\tau_1-\tau_3) - (\tau_1-\tau_3)^2\sigma^2/2} \\ &\quad \times e^{-\gamma(\tau_1+\tau_3)}, \end{aligned} \quad (7c)$$

$$\begin{aligned} R_6^{(3)}(\tau_1, \tau_2, \tau_3) &= -|\mu_{eg}|^2 |\mu_{fe}|^2 e^{-i\Delta\tau_3} e^{+i\omega_{eg}(\tau_1+\tau_3) - (\tau_1+\tau_3)^2\sigma^2/2} \\ &\quad \times e^{-\gamma(\tau_1+\tau_3)}, \end{aligned} \quad (7d)$$

where we have taken $\gamma_{eg} = \gamma_{fe} \equiv \gamma$, and we have suppressed the population-relaxation component, because the exponential term is

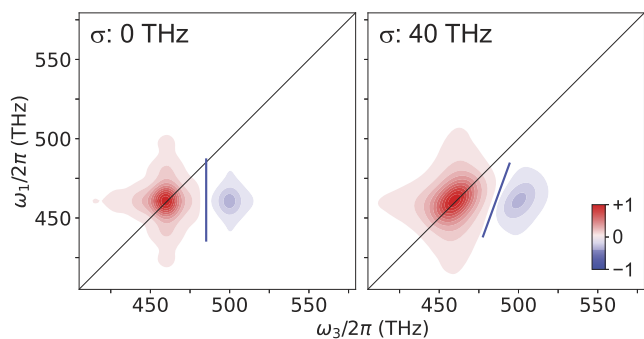


FIG. 1. Simulated, normalized 2D spectra using Eq. (7), with (right, $\sigma = 40$ THz) or without (left, $\sigma = 0$ THz) static inhomogeneous broadening. The static inhomogeneous broadening leads to a persistent diagonally tilted node between the excited-state absorption (blue) and ground-state bleach (red) signals. The solid blue line indicates the node.

common to all paths and only serves as a common amplitude factor that has no effect after normalization.

The expressions in Eq. (7) allow us to study the effects of inhomogeneous broadening in the presence of ESA signals that overlap the GSB signal. We choose a set of parameters that resemble the measured Cy5 spectra: $\omega_{eg} = 460$ THz, $\omega_{fe} = 500$ THz, $\mu_{fe} = 0.8\mu_{eg}$, and $\gamma = 40$ THz and then plot the simulated spectra in Fig. 1 for two distinct cases of static inhomogeneous broadening. The simulations reveal that static inhomogeneous broadening leads to a persistent diagonally tilted node between the ESA and GSB signals, and the lack of inhomogeneous broadening causes the node to be vertically orientated. In Sec. IV, we quantify the tilt of the node and use it as a proxy for the presence of static inhomogeneous broadening.

III. METHODS

A. Sample preparation

We purchased the carboxylic acid form of Cy5 from Lumiprobe and the Cy5 labeled and unlabeled 26-nucleotide (“nt”) DNA oligomers from Integrated DNA Technologies. Table I presents the DNA oligonucleotide sequences. The structure of Cy5 attached to the 5′ and 3′ sides of the DNA backbone was published previously,^{41,42} where there are two covalent bonds between the dye and DNA, created using phosphoramidite chemistry.^{43,44} The Cy5-C sequence is common to each of the DNA-templated monomers studied here. Sequence C has a high cytosine and guanine base content relative to sequences A, B, and D; higher cytosine and guanine content enhances the stability of the duplex, due to the stronger bonding between cytosine and guanine relative to adenine and thymine.⁴⁵ The ssDNA–Cy5 monomer solution incorporates the Cy5-C oligonucleotide only. The dsDNA–Cy5 monomer consists of the Cy5-C, hybridized with its complement C′. The HJ–DNA–Cy5 monomer consists of the four sequences, A, B, Cy5-C, and D, each of which have two domains complementary to two of the four sequences, such that a four-armed junction is the most energetically favorable structure.

We rehydrated the samples with ultrapure water (Barnstead Nanopure, Thermo Scientific) to produce a 100 μM stock solution and prepared Cy5-labeled double stranded DNA (dsDNA–Cy5) and four-armed Holliday junctions (HJ–DNA–Cy5), by combining equimolar amounts of complementary oligomers to the Cy5 labeled single-stranded DNA (ssDNA–Cy5) in a 1 \times TAE [40 mM tris(hydroxymethyl)aminomethane, 20 mM acetic acid, 1 mM ethylenediaminetetraacetic acid] buffer solution (pH 8.0) with 15 mM added magnesium chloride (MgCl_2), to obtain a final DNA concentration of 12 μM .⁴² The resulting solutions remained at room temperature for 24 h for hybridization and self-assembly to form the desired structure, and we conducted all measurements at room temperature.

For femtosecond measurements, the peak optical density (OD) of each sample was about 0.27 in a 1-mm path length cuvette (Starna 32-Q-1/UTWA2), and a magnetic stirrer (Ultrafast Systems) stirred the samples during all time-resolved spectroscopy measurements.

B. Steady-state spectroscopy

We used a Cary 5000 UV–Vis–NIR spectrophotometer (Agilent Technologies, Santa Clara, CA) and a Horiba Fluorolog 3

TABLE I. Oligonucleotide sequences, where “iCy5” stands for internally labeled Cy5.

Label	Sequence (5′–3′)	Length (nt)	Purification method
Cy5-C	CAC TCA CAT TCC A/iCy5/C TCA ACA CCA CAA	26	HPLC
C′	TTG TGG TGT TGA GT GGA ATG TGA GTG	26	Desalting
A	ATA TAA TCG CTC GCA TAT TAT GAC TG	26	Desalting
B	CAG TCA TAA TAT GTG GAA TGT GAG TG	26	Desalting
D	TTG TGG TGT TGA GCG AGC GAT TAT AT	26	Desalting

spectrofluorometer (Horiba Scientific, Edison, NJ) to collect the steady-state absorption and fluorescence spectra, respectively. We diluted samples for fluorescence measurements to a peak absorbance of <0.05 OD, and we obtained fluorescence quantum yield (FQY) values using a previously created reference sample²⁵ and a standard method.⁴⁶

C. Time-resolved laser spectroscopy

We measured fluorescence lifetimes of the dilute solutions using a time-correlated single photon counting (TCSPC) spectrometer (PicoQuant FluoTime 250). The instrument response function (IRF) for the light source exciting at 594 nm was ~60 ps. The coefficients of determination (R^2) for a single-exponential fit after the IRF time were 0.9987, 0.9983, 0.9995, and 0.9993 for the free Cy5, ssDNA–Cy5, dsDNA–Cy5, and HJ–DNA–Cy5 samples, respectively.

The output of a commercial 1 kHz amplified Ti:sapphire laser (Coherent Astrella), producing ~100 fs pulses, centered at 796 nm, pumped a home-built noncollinear optical parametric amplifier (NOPA), which is identical to the one used in prior works.^{47–50} The ultra-broadband laser pulses spanned ~500 to 800 nm, and the shot-to-shot stability was about 1% relative standard deviation.⁵¹ A shortpass filter (Optosigma SHPF-25C-770) removed the residual fundamental at wavelengths longer than ~750 nm, and a dispersion-compensating mirror pair (Novanta Laser Quantum DCM9) adjusted the temporal dispersion of the pulse, which had a duration of <9 fs based on transient-grating frequency-resolved optical gating measurements,⁵² conducted using a 1-mm thick Infrasil window (Thorlabs). Figure 3 shows the spectrum of the NOPA laser pulse.

The four-wave mixing spectrometer replicated an instrument detailed previously^{47–49} and was motivated by prior instruments.^{53,54} Briefly, two computer-controlled delay stages (Newport XMS50-S, XMS160-S) adjusted the relative timing of four pulses arranged in the BOX geometry. The electronics package for dual-chopper balanced detection included two phase-locked, rotary optical choppers (New Focus 3502), a data-acquisition board (NI PCI-6281), and an amplified, silicon-based photoreceiver (New Focus 2001-FS).^{55,56} The spectrally resolved detector consisted of an Andor Shamrock 163 and Zyla 5.5 sCMOS camera, calibrated to an estimated ± 1 nm, using a linear fit to multiple peaks from an atomic lamp. We used two quarter-area, ND 2.0 filters, each 0.25 mm-thick UV fused silica, to attenuate the local oscillator power by a factor of 10^4 in the 2D ES measurements. The energy of each excitation beam was ~40 nJ/pulse, and the spot size was ~80 μm in 2D ES measurements.

We report the spectra as normalized transient transmittance, $\Delta T/T$, as a function of frequency (THz). We evaluated the fidelity of the instrument by measuring cresyl violet perchlorate—a laser dye that has become a reference standard for evaluating newly constructed femtosecond spectrometers.⁵⁷ The phase stability of the interferometer was $\sim \Lambda/500$, under conditions replicating a 2D measurement of cresyl violet at $\tau_1 = 0$, $\tau_2 = 10$ ps. We collected each 2D spectrum by scanning the coherence time, τ_1 , from 0 to 70 fs in 2 fs steps for each population time, τ_2 , which we stepped from 0.01 to 1000 ps in 11 logarithmic steps in the Cy5 measurements. We display the real part of the total spectrum arising from the sum of the rephasing and nonrephasing signals.⁵⁸

We performed the spectrally resolved transient-absorption reference measurements required for “phasing” the spectra immediately after performing the 2D measurements, by making only three physical adjustments to the spectrometer. The first was to block two of the excitation beams, and the second was to adjust the energy of the remaining excitation beam to be equal to the total of the three excitation beams in the 2D measurements. The third change was to rotate one of the quarter-area ND 2.0 filters such that it remained in the path of both beams, but no longer attenuated the probe beam; this maintained the dispersion while attenuating the probe from 10^4 to 10^2 to increase the signal-to-noise ratio.

We used the curve fit functionality of Python and SciPy to “phase” the 2D spectra, which means to determine each coefficient c_k of a Taylor expansion of the phase function

$$\phi(\omega_3) = \sum_{k=0} c_k \omega_3^k, \quad (8)$$

which minimizes the difference, $\Delta(\tau_2)$, between the normalized transient-transmittance spectrum, $S_{\text{TT}}(\tau_2, \omega_3)$, and the normalized projection of the 2D spectrum onto the emission frequency axis, $P_{2\text{D}}(\tau_2, \omega_3)$,^{27,59,60}

$$\Delta(\tau_2) = S_{\text{TT}}(\tau_2, \omega_3) - P_{2\text{D}}(\tau_2, \omega_3), \quad (9)$$

where

$$P_{2\text{D}}(\tau_2, \omega_3) = \text{Re} \left\{ \int S_{2\text{D}}(\omega_1, \tau_2, \omega_3) e^{-i2\pi\phi(\omega_3)} d\omega_1 \right\}. \quad (10)$$

For each τ_2 value, we compute the error between the projected 2D spectrum and its corresponding transient-transmittance spectrum using the coefficient of determination

$$R^2(\tau_2) = 1 - \frac{\int (S_{TT}(\tau_2, \omega_3) - P_{2D}(\tau_2, \omega_3))^2 d\omega_3}{\int (S_{TT}(\tau_2, \omega_3) - \overline{S_{TT}}(\tau_2, \omega_3))^2 d\omega_3}, \quad (11)$$

where $\overline{S_{TT}}(\tau_2, \omega_3)$ is the mean of the measured transient-transmittance spectrum. The fitting algorithm achieved $R^2 > 0.99$ for all measurements.

D. Computational methods

1. DFT methods

We performed all density functional theory (DFT) and time-dependent (TD-) DFT calculations using Gaussian16 software.⁶¹ First, we optimized the ground-state geometries using the M06-2X functional⁶² with the 6-31+G(d,p) basis set to a residual force of 4.5×10^{-4} Hartree/Bohr. We then performed vertical excited-state calculations to the lowest seven excited states. We used the integral equation formalism polarizable continuum model (IEFPCM)^{63,64} to solvate the Cy5 molecules in water, assuming nonequilibrium conditions for the excited-state calculations.

2. MD methods

We performed molecular dynamics (MD) simulations of a free Cy5 dye in solution, a Cy5 dye attached to ssDNA, and a Cy5 dye attached to dsDNA, using the DNA sequences shown in Table I, with the GROMACS 2022.2 software package.⁶⁵ We used the OL15 force-field^{66,67} with non-bonded modifications⁶⁸ for the DNA bonded and non-bonded parameters and the general amber force-field (GAFF)⁶⁹ for the Cy5 bonded and van der Waals parameters. To calculate the atomic point charges of Cy5, we applied the restrained electrostatic potential (RESP) fitting method,⁷⁰ using the electrostatic potential calculated at the HF/6-31G* theory level. We built the initial dye-DNA structures using the UCSF ChimeraX software.⁷¹

We used the TIP3P water model⁷² in a truncated octahedral box, ensuring a 1.2 nm separation between the dye/dye-DNA structure and box edge, neutralized the system's Mg^{2+} and Cl^- ions, and included an excess $MgCl_2$ concentration of 15 mM. We utilized neighbor-searching, with a cutoff of 1.2 nm, limited the Van der Waals interaction to 1.2 nm, and implemented the Particle Mesh Ewald (PME) method with a real-space Coulomb cutoff of 1.2 nm. The LINCS algorithm was used to constrain the bonds to the hydrogen atoms.⁷³

To prepare the systems for MD simulations, we first energy-minimized the structures with the steepest descent method for 1000 steps. Second, we ran two 1 ns equilibration steps, with harmonic constraints of 1000 kJ/(mol nm²) for the first step and 100 kJ/(mol nm²) for the second step, applied to heavy atoms, keeping the number of atoms, volume, and temperature constant. A third step was performed with no constraints. We then performed MD simulations for 500 ns at 1 atm and 300 K, keeping the number of atoms, pressure, and temperature constant, with a timestep of 2 fs. We utilized the velocity-rescale thermostat⁷⁴ with a coupling time of 0.1 ps and the Parrinello–Rahman barostat⁷⁵ with a coupling time of 1.0 ps. Datasets arose from three replicas, each with different initial velocities, for each system, where we treated the first 50 ns of each replica as an equilibration period that was not used for data analysis. Figure 2 details the parameters used to quantify dye conformations.

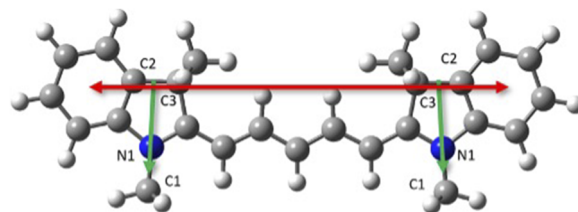


FIG. 2. The vectors used to calculate the angle between the two ends of the Cy5 dye are shown in green, and the vector representing the length of the Cy5 dye is shown in red. The green vectors were determined by calculating the unit vector connecting the atoms labeled N1 and C1 to the C2 and C3 atoms for both ends. The length of the Cy5 dye was calculated using the centers of mass of the atoms in the two aryl rings at either end of the Cy5 dye.

IV. RESULTS AND DISCUSSION

As a first step to obtaining information provided by the Cy5 dye about the DNA structures, we analyzed the steady-state spectra and the photophysical properties of the four samples. Table II lists the properties based on the spectra displayed in Fig. 3 and TCSPC measurements. The data reveal two key trends. The first is that attachment to DNA redshifts the steady-state absorption and fluorescence spectra by up to 10 nm relative to the free dye that was in the aqueous buffer solution. Prior reports presented evidence supporting the hypothesis that this redshift is due to a solvatochromic effect caused by differences in solvation polarity.^{76–78}

To support this hypothesis further, we tested the competing hypothesis that the redshift is caused by a change in conjugation due to the use of dual phosphoramidite linkers to attach the Cy5 dye to the DNA. We, therefore, performed DFT computations of Cy5, with and without its linkers, using a polarizable continuum model of water as the solvent. After equilibrating the ground-state geometry, we computed the excitation energies and oscillator strengths for each structure. The optimized molecular structures of the Cy5 dyes, with and without linkers, are shown in Fig. 4. The two computations yielded values that were identical to within ~1% for the seven lowest-energy excited states, which were singlets. For example, the lowest-energy transition was 517.4 nm (515.8 nm) with (without) the linkers. These computational results are not consistent with the extended-conjugation hypothesis, and, therefore, the solvatochromism mechanism is further supported.

The second major trend present in the tabulated data is that the excited-state lifetime is increased when the dye is attached to DNA. This also has been observed previously; Lee *et al.* showed that DNA attachment enhances photostability of cyanine dyes.²⁰ Here, we also measured the fluorescence quantum yield (FQY) values, and there is an increase in this value concomitant with the increase in the excited-state lifetime. To gain additional insight into the photophysics of each sample, we further calculated the radiative and nonradiative decay rate constants from the measured lifetime and FQY values.⁷⁹ Keeping in mind that each sample could be a heterogeneous mixture of conformers, we glean three key observations from these results: (i) The radiative decay rate of the free Cy5 solution is the largest, while that of the dsDNA–Cy5 solution is the smallest. (ii) The nonradiative decay rate of the free Cy5 solution is 4–5× larger than that of any DNA–Cy5 solution. (iii) The

TABLE II. Steady-state and photophysical parameters of Cy5 samples; lifetimes, fluorescence quantum yields (FQYs), and radiative and nonradiative decay rates.

Sample	Absorption max (nm)	Fluorescence max (nm)	Stokes shift (THz)	Lifetime (ns)	FQY (%)	Calculated decay rates	
						Radiative (ns^{-1})	Nonradiative (ns^{-1})
Free Cy5	640	660	14.2	0.6	18	0.30	1.40
ssDNA-Cy5	648	670	15.2	1.8	45	0.25	0.31
dsDNA-Cy5	646	665	13.3	1.7	36	0.21	0.38
HJ-DNA-Cy5	651	670	13.1	2.1	48	0.23	0.25

nonradiative decay rate of the dsDNA-Cy5 solution is the largest of the DNA-Cy5 solutions. That free Cy5 (dsDNA-Cy5) has the largest (smallest) radiative decay rate indicates that it has the largest (smallest) absorption strength, given the relationship between these parameters established by Strickler and Berg,⁸⁰ which we further infer to indicate that the transition dipole moment amplitude of free Cy5 (dsDNA-Cy5) is the largest (smallest). These results are consistent with the notion that free Cy5 primarily adopts a mostly all-trans, planar configuration in the solution, whereas the solution of dsDNA-Cy5 may consist of either a more *cis*-like, twisted configuration or a mixture of *cis* and *trans* conformers. That the nonradiative decay rate of free Cy5 is the largest is consistent with the expectation that nonradiative decay, which is primarily mediated in these samples by bond rotation following photoexcitation, would be minimized in samples of Cy5 bicovalently attached to

DNA. Finally, the unexpectedly large nonradiative decay rate of the dsDNA-Cy5 sample (compared to the ssDNA-Cy5 and HJ-DNA-Cy5 samples) is consistent with the interpretation proposed above, wherein the molecules in the solution adopt a more *cis*-like, twisted configuration, which is expected to facilitate nonradiative decay. The data in Table II, therefore, reveal that attaching Cy5 to DNA changes the solvation environment, causing a spectral redshift, and can promote a more *cis*-like, twisted configuration, causing a decrease and increase in radiative and nonradiative decay rates, respectively.

Interestingly, despite the redshift and lifetime trends, there is no discernible trend in the Stokes shift values relative to that of the free dye. The Stokes shift is a single value that describes the collective energy losses due to solvent reorganization and intramolecular and intermolecular vibrational relaxation.^{81,82} Because a trend is not observed, this reveals that the vibronic coupling environment is not

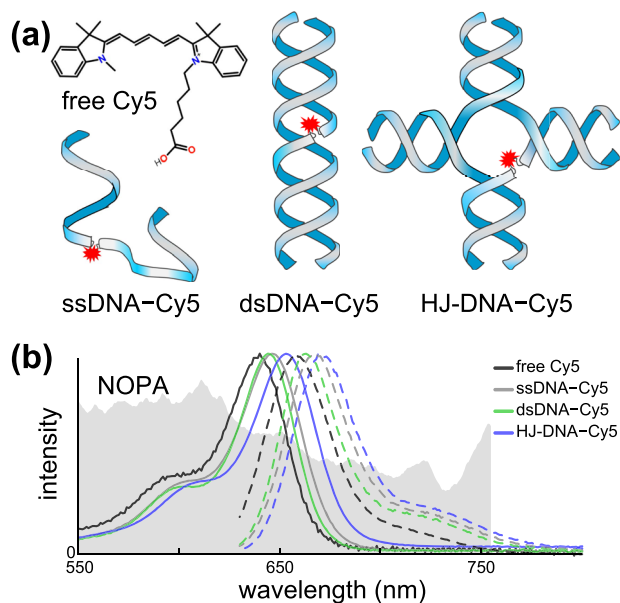


FIG. 3. Sample structures and spectra. (a) Illustration of structures, where red star represents the Cy5 molecule that is bicovalently attached to each DNA nanostructure. The HJ illustration is not intended to represent a specific conformer. (b) Absorption (solid) and fluorescence (dashed) spectra of the samples with the laser pulse spectrum (NOPA; shaded area).

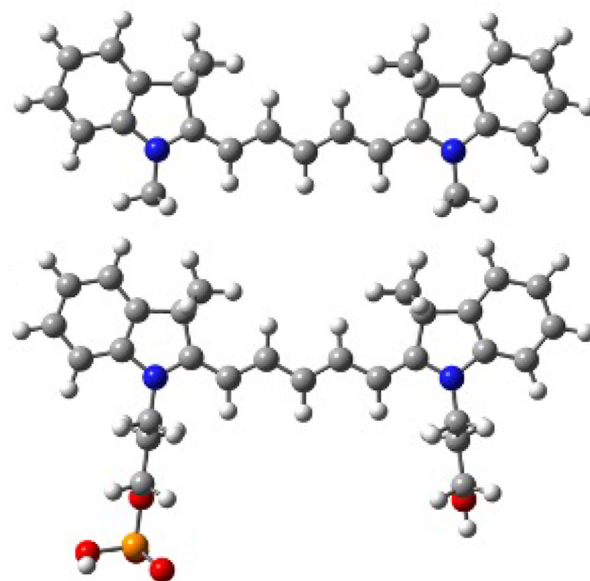


FIG. 4. DFT-optimized molecular structure of Cy5, with (bottom) and without (top) linkers. Bonds connecting the Cy5 to the linkers or the linkers to the DNA were capped with H atoms. Gray, white, blue, red, and yellow represent the C, H, N, O, and P atoms, respectively.

altered systematically by the attachment to the DNA. Indeed, the intensities of the vibronic shoulders present in the absorption and fluorescence spectra in Fig. 3 are qualitatively similar among all samples.

The conventional spectroscopic characterization methods did not provide detailed insight into the conformational distribution of the DNA macromolecules, and, therefore, we turn to the advanced spectroscopic tool of 2D ES. Here, we use a fundamental aspect of the spectroscopic method—its phase-correlation property via the photon echo²⁸—to gain insight into the structural properties of DNA, by evaluating the line shapes of peaks in the 2D spectra of the Cy5 dye. Researchers have used line shape studies in 2D spectroscopy to probe many properties,⁸³ including spectral diffusion⁸⁴ and the dynamic Stokes shift.⁸² These studies rely on the dynamic changes in the shapes of peaks in a 2D spectrum that can occur as the waiting time (τ_2) evolves. A 2D spectrum correlates the *phase* of each excitation frequency to that of each emission frequency. The information about these correlations is embedded in the shape of a peak in a real-valued 2D correlation spectrum.⁵⁸ In such a spectrum, the true line shape of a transition is given by the antidiagonal

linewidth of a peak.^{34,85} This is often known as ‘homogeneous’ broadening, because it refers to the instantaneous fluctuations that inherently broaden a transition. For a condensed-phase sample, this will depend on factors such as the solvent and temperature. In addition to the homogeneous linewidth, some peaks will have a persistent diagonal elongation. In 2D studies, diagonal elongation of the ground-state bleach (GSB) peak that persists to very long (nanosecond) timescales is often referred to as “inhomogeneous” broadening, to distinguish it from homogeneous broadening. Such persistent diagonal elongation implies that there is a microscopic mechanism that prevents dyes excited by high-frequency light from exploring environments or configurations that would be excited by low-frequency light, and vice versa. In some samples, the inhomogeneous line-shape has a straightforward physical explanation. For example, a colloidal semiconductor-nanocrystal sample is a collection of nanocrystals of varying sizes, and the transition energy depends on the size of the nanocrystal.⁸⁶ The nanocrystals cannot change sizes, and, therefore, the line shape remains inhomogeneously broadened at all waiting times.⁶⁰ In the DNA–Cy5 samples studied here, we would interpret any inhomogeneously broadened peaks as arising

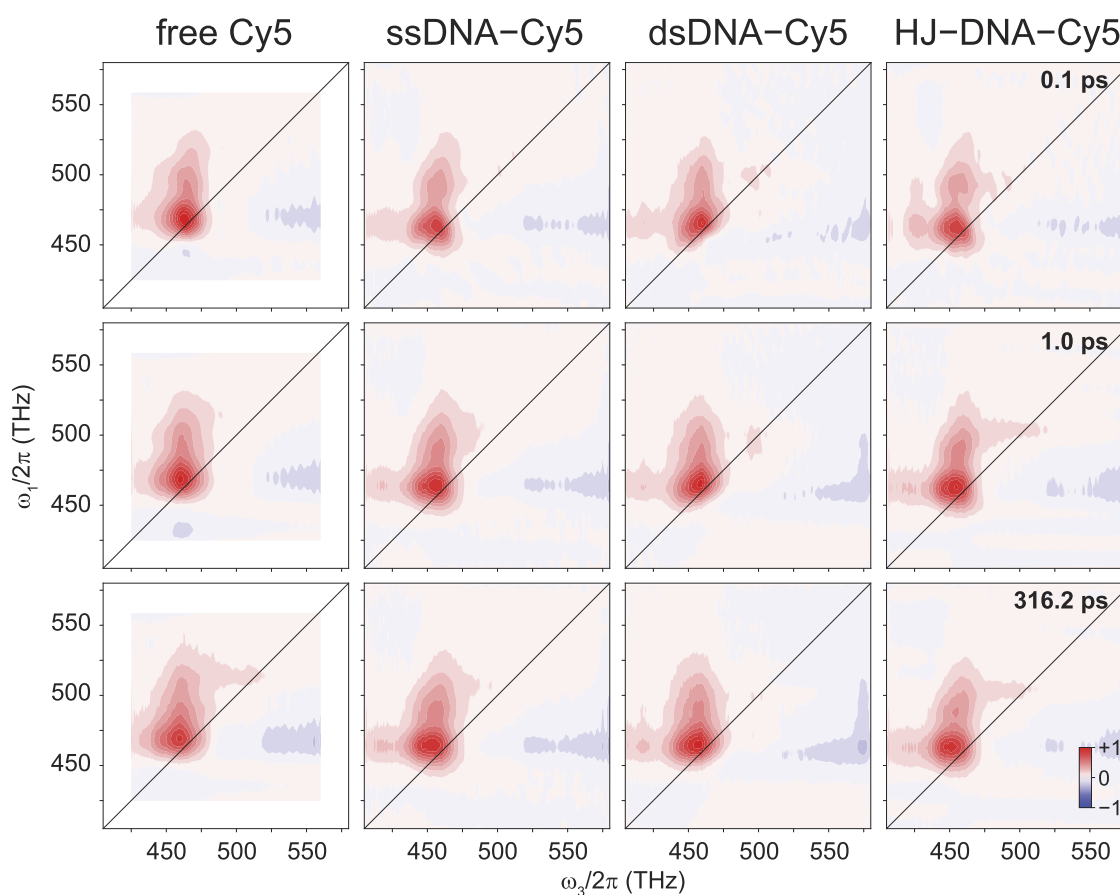


FIG. 5. Normalized room-temperature 2D ES of the four samples at indicated waiting times. The spectra of free Cy5 were truncated slightly to attain adequate ($R^2 > 0.99$) phasing.

from the DNA, preventing the dye from exploring energetically distinct conformations or solvent configurations throughout the duration of the measurement, which is 1 ns. The discussion above applies to an idealized two-level system. Other molecular and spectroscopic properties, such as the dynamic Stokes shift, vibrational coherences, and the presence of overlapping excited-state absorption pathways, can complicate the analysis and interpretation.

We present the normalized room-temperature 2D spectra of the four Cy5 monomer samples in Fig. 5 at representative waiting time values of 100 fs (top row), 1 ps (middle row), and 316.2 ps (bottom row). The peaks in the 2D spectra of the DNA–Cy5 samples present one issue that complicates a seemingly straightforward line shape study: The primary GSB signal that one would typically analyze is overlapped by an ESA peak. Indeed, the region surrounding the main peak at an emission frequency of about 475 THz appears to have zero signal. This lack of signal appears in the reference TA spectrum, see the Appendix, but the absolute-value 2D spectrum—although it does not have a physical interpretation in a line shape study—does show high amplitude in this region. This distinction reveals that the region of zero signal in the TA and real-valued 2D spectra arises from significant interference between the GSB and ESA signals, which have opposite signs. Because the GSB peak is not isolated, we cannot use a typical analysis method, such as the center line slope method.^{83,87,88} Instead, here, we analyze a distinct spectral feature that will also contain the same information about correlations between excitation and emission frequencies. Specifically, we analyze the slope of the node that forms between the GSB and ESA features. To do this, for each value of τ_2 , we selected a specific ω_1 slice through the 2D spectrum and identified the ω_3 value that was the minimum of the absolute values of the real-valued 2D spectrum

$$\omega_3^{\min} = \min \left(\left| \operatorname{Re} \{ S_{2D}(\omega_1, \tau_2, \omega_3) \} \right|_{(\omega_1, \tau_2)} \right). \quad (12)$$

This yielded a set of about 20 $(\omega_3^{\min}, \omega_1)$ coordinate pairs, which we then fit to a linear function. To remove the singularity that would arise at a perfectly vertical node, we interchange the dependent and independent variables to compute the *inverse* slope, χ ,

$$\omega_3^{\min} = \omega_1 \chi + \omega_b, \quad (13)$$

where ω_b is the intercept of the linear fit. Figure 6(a) shows an example fit for the dsDNA–Cy5 sample at 316.2 ps waiting time. Panel (b) in Fig. 6 illustrates the cases most relevant to this report, which are $\chi = 0$ and $\chi = 1$. An inverse slope of $\chi = 0$ indicates a completely vertical line, which indicates no phase memory (correlation) among the lower and higher frequencies. An inverse slope of $\chi = 1$ would indicate a node that is parallel to the diagonal. Figure 6(c) shows the values of χ for each sample across four decades of waiting time. Error bars represent one standard deviation of the fit error. Due to the nonresonant response,⁸⁹ we omitted the 2D spectra acquired at waiting times of 10 and 31 fs from this analysis. Additionally, there are non-negligible vibrational quantum beats that take ~ 250 fs to dissipate,⁹⁰ and, thus, some of the spectra at 100 and 316 fs have large errors. Due to its short lifetime, the 1 ns measurement of free Cy5 had a weak signal, which led to a relatively large error. Some values in Fig. 6(c) are negative, which, in principle, indicates a negative

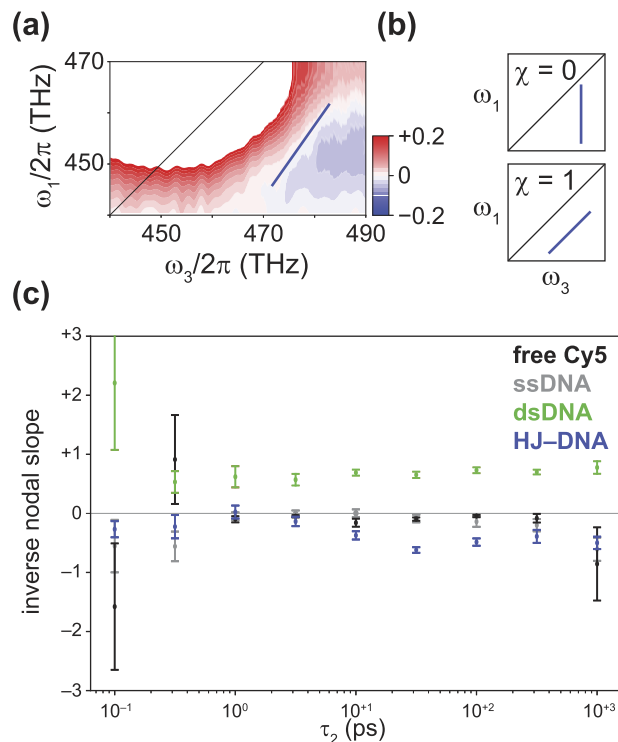


FIG. 6. (a) Fitted region of 2D ES of dsDNA–Cy5 sample at 316.2 ps. Contours drawn at 1% intervals over the bounds of $\pm 20\%$. The dark blue line indicates the linear fit to the node. (b) Illustrations of cases $\chi \in \{0, 1\}$. (c) Inverse slope of the nodal line between GSB and ESA features, χ , for all samples across four decades of waiting time (τ_2).

correlation between the excitation and emission frequencies. However, most of the negative inverse slope values also have very large uncertainties, indicating that these values likely arise from noise. Mechanisms including vibrational coherences, pulse chirp, and the dynamic Stokes shift could, in principle, induce a negative-valued inverse nodal slope; however, this effect is outside the scope of the current study, and most of the negative values are omitted from the detailed analysis below.

A cursory inspection of the data presented in Fig. 6(c) qualitatively reveals that the dsDNA–Cy5 sample has $\chi \sim 1$, whereas the other three samples have $\chi \sim 0$ across all four decades of measured waiting time. More quantitatively, the time-averaged χ values for each sample are: -0.22 ± 0.24 for free Cy5, -0.24 ± 0.14 for ssDNA–Cy5, $+0.84 \pm 0.15$ for dsDNA–Cy5, and -0.33 ± 0.13 for HJ–DNA–Cy5. These non-zero inverse slopes of the dsDNA–Cy5 reveal that dsDNA prevents the bicovalently bound Cy5 dye from exploring all possible energetically distinct configurations in this spectral region within 1 ns, and this contrasts with the other three samples, wherein the dye can explore all energetically distinct configurations in this spectral region within about 1 ps. Because the dye is a cyanine dye with a conjugated methine bridge chain having multiple conjugated carbon–carbon bonds, one can hypothesize that the dsDNA locks the dye into certain preferred isomers or conformers in their ground states, and neither thermal fluctuations nor

photoexcitation is adequate to induce isomerization of appreciable yield within the measurement time.

To test the hypothesis regarding multiple conformers, we conducted MD simulations on the ground electronic state of free Cy5, ssDNA–Cy5, and dsDNA–Cy5. The HJ–DNA–Cy5 system was not amenable to computational study because of its size. The simulations ran for 500 ns. For each frame (10 ps), we quantified the angle between the ends of the dye, θ_e , and the length of the dye to produce a two-dimensional histogram of occurrences. Each histogram in Fig. 7 shows multiple preferential conformers of the dye. We extracted the parameters for these preferential conformers and tabulated them in Table III, and we also produced a visual image of each conformer and displayed it in the bottom of Fig. 7. The most common configuration for the ground-state structure of the Cy5 dye in all three environments is the trans, syn (planar) conformer, which is characterized by $\theta_e \sim 8^\circ$ and dye length of 1.37 nm and is highlighted by the blue circle in Fig. 7. Free Cy5 is also found—to a lesser extent—in the trans, anti (planar) and cis, anti (planar) conformers. Free Cy5 is rarely found in a twisted configuration. The MD results reveal that ssDNA provides a microscopic environment that is even more likely to avoid the two twisted conformers. Indeed, inspecting

the simulation frames reveals that the flexibility and coiling of the ssDNA strand leads to stacking of the Cy5 with the nucleobases and a lack of significant secondary conformers. By contrast, the secondary conformers of Cy5 in the dsDNA environment are twisted, and the MD simulation frames show that the dye is located primarily on the outside of the double-stranded DNA base region. Because the only relevant DNA–dye interactions on the outside of the double helix are the two phosphoramidite linkers, the dual linkers may prevent the formation of either anti (planar) structure, by restricting the amount of twisting of the dye; to form an anti conformer and to remain bivalently bonded to the DNA, the linkers would have to stretch much more than if the dye simply remained in the trans, syn (planar) or one of the twisted conformers.

The MD results reveal that ssDNA leads to flexibility and nucleobase stacking that strongly biases Cy5 to be primarily in the trans, syn (planar) conformer. By contrast, the Cy5 molecule attached to dsDNA is exterior to the helix and has two key secondary conformers, both twisted. The 2D spectra suggest that one of the secondary conformers in dsDNA–Cy5 would have a transition frequency within about 10–20 THz of the dominant conformer, which would be adequate to cause significant spectral overlap, but

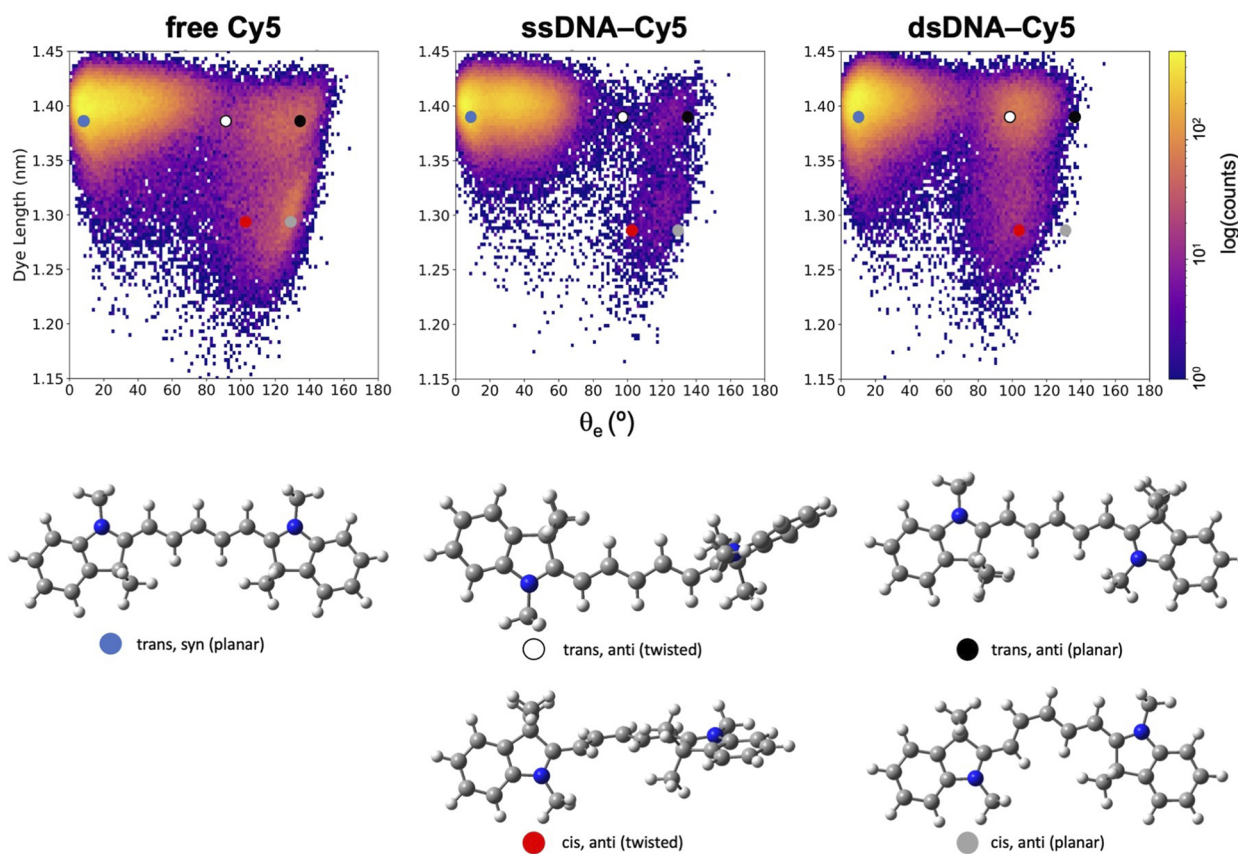


FIG. 7. (top) Two-dimensional histograms from MD simulations for free Cy5, ssDNA–Cy5, and dsDNA–Cy5 (bottom) The five representative Cy5 conformers found in the MD simulations, as marked in each histogram by colored circles.

TABLE III. Parameters of five key Cy5 dye conformations from MD simulations.

Conformer	Dye length (nm)	θ_e (deg)
Trans, syn (planar)	1.37	8
Trans, anti (twisted)	1.37	90
Trans, anti (planar)	1.37	134
cis, anti (planar)	1.28	128
cis, anti (twisted)	1.28	99

not be completely degenerate and, thereby, would cause no line broadening. To support this interpretation, one could, in principle, compute the transition frequency of each conformer; however, previous studies have observed that cyanine dyes present a computational challenge.^{91,92} Future work will include calculating the transition frequencies of the predicted dye conformers, with particular focus on how the exchange-correlation functional, solvent environment, and other relevant computational parameters affect the electronic structure of the DNA-templated dye.

Combined, the 2D ES and MD results reinforce the conclusion that dsDNA provides an environment for the dye that is unique within the series of DNA structures studied here. Indeed, considering only the primary electronic transition, the 2D ES measurements demonstrate that the environments around the dye in both ssDNA and HJ-DNA are more similar to that of the dye free in solution than to that of the dye in dsDNA. This was unexpected, not only because the configurational space of Cy5 when attached to ssDNA is more limited than that of both free Cy5 and dsDNA-Cy5, but also because, in ssDNA-Cy5, there is base-pair stacking, which is not possible in the free Cy5 solution. Evidence from literature also suggests that this base-pair stacking is possible in HJ-DNA for Cy5 dimers,⁹³ which may also apply for a Cy5 monomer. By contrast, the results, here, from 2D spectroscopy—which can reveal conformations that affect the transition frequency—show that the rigidity of dsDNA locks the dye into two or more subensembles that have non-degenerate transition frequencies, causing peaks to overlap in a way that leads to inhomogeneous broadening, observed as the persistent diagonal elongation in the 2D spectrum. The MD simulations indicate that the non-degenerate subensemble consists of twisted conformations of Cy5 that are not present to an appreciable extent in the free Cy5 or ssDNA simulations. Such behavior may be related to the rigid, organized, helical nature of dsDNA, discussed further by Asanuma *et al.* in their seminal review.⁹⁴

V. CONCLUSIONS

In this report, we have analyzed steady-state and femtosecond 2D electronic spectra of Cy5 monomers, either free in aqueous solution or bivalently bound to three distinct DNA structures, with an aim of extracting information about the DNA conformations. Due to overlapping spectral features, we modified the conventional line shape analysis to quantify the slope of the node that arose between the ground-state bleach and excited-state absorption features. The 2D spectra revealed that ssDNA and HJ-DNA environments for the dye were similar to that of aqueous solvation. In these three environments, there was no correlation between excitation and emission

frequencies in the spectral feature of interest. This indicated that the dye was in one dominant conformation relevant to this spectral window. In contrast, the 2D spectra of dsDNA revealed a strong correlation between excitation and emission frequencies that persisted throughout the duration of the measurement. This signature of inhomogeneous broadening indicates that, in dsDNA, the dye is present in more than one conformer and is not able to explore all energetically distinct environments within the duration of the measurement. The MD simulations supported these findings and provided further insights into the specific nature of the structures. These results provide more context to DNA's structural heterogeneity, relevant to optical probes in spectroscopy and microscopy studies.

ACKNOWLEDGMENTS

The DOE, Office of Basic Energy Sciences, Division of Materials Science and Engineering, through the Established Program to Stimulate Competitive Research (EPSCoR), via Award No. DE-SC0020089, wholly supported this research, except as follows: The Department of the Navy, Office of Naval Research (ONR), via ONR Award No. N00014-19-1-2615, supported the construction of the two-dimensional electronic spectrometer, DFT calculations, and MD simulations.

AUTHOR DECLARATIONS

Conflict of Interest

The authors have no conflicts to disclose.

Author Contributions

Matthew S. Barclay: Data curation (equal); Investigation (equal); Methodology (equal); Writing – review & editing (equal). **Azhad U. Chowdhury:** Investigation (equal). **Austin Biaggne:** Conceptualization (equal); Data curation (equal); Methodology (equal); Software (equal); Writing – original draft (equal); Writing – review & editing (equal). **Jonathan S. Huff:** Investigation (equal); Writing – review & editing (equal). **Nicholas D. Wright:** Investigation (equal); Writing – review & editing (equal). **Paul H. Davis:** Funding acquisition (equal); Writing – review & editing (equal). **Lan Li:** Funding acquisition (equal); Software (equal); Writing – review & editing (equal). **William B. Knowlton:** Funding acquisition (equal). **Bernard Yurke:** Funding acquisition (equal); Writing – original draft (equal). **Ryan D. Pensack:** Conceptualization (equal); Funding acquisition (equal); Methodology (equal); Project administration (equal); Writing – review & editing (equal). **Daniel B. Turner:** Conceptualization (equal); Data curation (equal); Formal analysis (equal); Funding acquisition (equal); Investigation (equal); Methodology (equal); Software (equal); Supervision (equal); Validation (equal); Writing – original draft (equal); Writing – review & editing (equal).

DATA AVAILABILITY

The data that support the findings of this study are available from the corresponding author upon reasonable request.

APPENDIX: PHASING OF 2D SPECTRA

Following the suggested specifications for newly constructed 2D spectrometers,⁵⁷ here, in Fig. 8, we report a representative example of the phasing accuracy. Phasing corrects subwavelength errors in pulse timings, imbalance between the rephasing and nonrephasing signals, as well as the pulse chirp, that mixes the absorptive and dispersive components of the signal.^{59,95} The blue trace is the reference spectrally resolved TA measurement, $S_{TT}(\tau_2, \omega_3)$, conducted immediately after the 2D scans of this sample, at an equivalent excitation power. The dashed orange trace represents the projection of the 2D spectrum, $P_{2D}(\tau_2, \omega_3)$, at this same waiting time, with optimized phase function applied. The green trace represents the residual, $\Delta(\tau_2)$, see Eqs. (9) and (10). Via Eq. (11), this dsDNA–Cy5 2D spectrum at 316.2 ps yielded an $R^2 = 0.996$. The gray trace in the bottom panel is the phase function, $\phi(\omega_3)$, applied to the complex-valued 2D spectrum, to achieve the match to the reference TA spectrum.

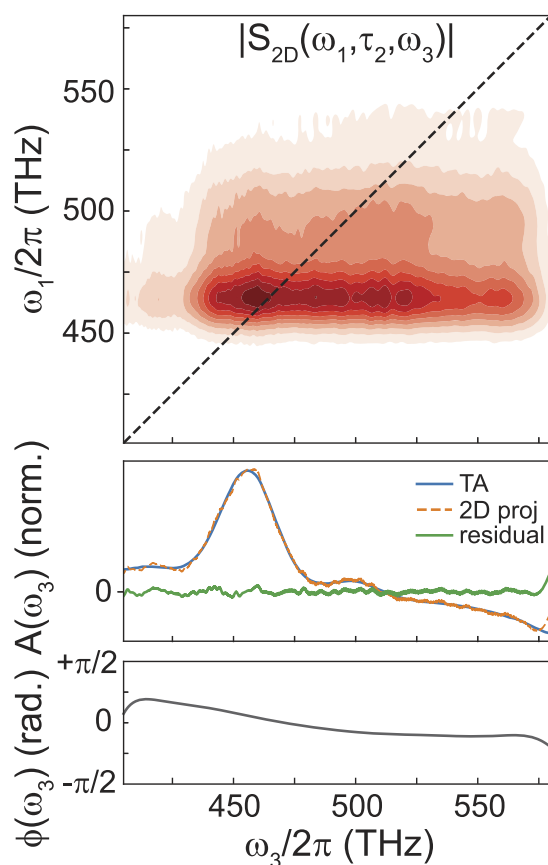


FIG. 8. (Top) Magnitude 2D ES. (Middle) Demonstrating phasing accuracy by comparing the projected real-valued 2D spectrum to its reference TA spectrum. (Bottom) Phase function applied to the complex-valued 2D spectrum in the top panel, to achieve a match between the 2D projection and the reference TA spectrum.

REFERENCES

- 1 P. H. von Hippel, N. P. Johnson, and A. H. Marcus, "Fifty years of DNA 'breathing': Reflections on old and new approaches," *Biopolymers* **99**, 923–954 (2013).
- 2 N. C. Seeman, "From genes to machines: DNA nanomechanical devices," *Trends Biochem. Sci.* **30**, 119–125 (2005).
- 3 F. C. Simmel, B. Yurke, and H. R. Singh, "Principles and applications of nucleic acid strand displacement reactions," *Chem. Rev.* **119**, 6326–6369 (2019).
- 4 P. Chidchob and H. F. Sleiman, "Recent advances in DNA nanotechnology," *Curr. Opin. Chem. Biol.* **46**, 63–70 (2018).
- 5 S. Nummelin, J. Kommeri, M. A. Kostiaainen, and V. Linko, "Evolution of structural DNA nanotechnology," *Adv. Mater.* **30**, 1703721 (2018).
- 6 X. Yan, S. Huang, Y. Wang, and Y. Tian, "Bottom-up self-assembly based on DNA nanotechnology," *Nanomaterials* **10**, 2057 (2020).
- 7 H. Ramezani and H. Dietz, "Building machines with DNA molecules," *Nat. Rev. Genet.* **21**, 5–26 (2020).
- 8 D. Y. Zhang and G. Seelig, "Dynamic DNA nanotechnology using strand-displacement reactions," *Nat. Chem.* **3**, 103–113 (2011).
- 9 Y. Zhang, V. Pan, X. Li, X. Yang, H. Li, P. Wang, and Y. Ke, "Dynamic DNA structures," *Small* **15**, 1900228 (2019).
- 10 M. DeLuca, Z. Shi, C. E. Castro, and G. Arya, "Dynamic DNA nanotechnology: Toward functional nanoscale devices," *Nanoscale Horiz.* **5**, 182–201 (2020).
- 11 S. Cao, F. Wang, L. Wang, C. Fan, and J. Li, "DNA nanotechnology-empowered finite state machines," *Nanoscale Horiz.* **7**, 578–588 (2022).
- 12 Y. Zhan and G. Zocchi, "Flexibility of DNA/PNA, DNA/LNA, DNA/RNA hybrids measured with a nanoscale transducer," *Europhys. Lett.* **119**, 48005 (2017).
- 13 C. Lee, K. S. Kim, Y.-J. Kim, J. Y. Lee, and D.-N. Kim, "Tailoring the mechanical stiffness of DNA nanostructures using engineered defects," *ACS Nano* **13**, 8329–8336 (2019).
- 14 R. Saran, Y. Wang, and I. T. S. Li, "Mechanical flexibility of DNA: A quintessential tool for DNA nanotechnology," *Sensors* **20**, 7019 (2020).
- 15 S. K. Roy, O. A. Mass, D. L. Kellis, C. K. Wilson, J. A. Hall, B. Yurke, and W. B. Knowlton, "Exciton delocalization and scaffold stability in bridged nucleotide-substituted, DNA duplex-templated cyanine aggregates," *J. Phys. Chem. B* **125**, 13670–13684 (2021).
- 16 K. Okamoto and Y. Sako, "State transition analysis of spontaneous branch migration of the Holliday junction by photon-based single-molecule fluorescence resonance energy transfer," *Biophys. Chem.* **209**, 21–27 (2016).
- 17 T. Ha, A. G. Kozlov, and T. M. Lohman, "Single-molecule views of protein movement on single-stranded DNA," *Annu. Rev. Biophys.* **41**, 295–319 (2012).
- 18 R. Roy, S. Hohng, and T. Ha, "A practical guide to single molecule FRET," *Nat. Methods* **5**, 507–516 (2008).
- 19 C. Joo, H. Balci, Y. Ishitsuka, C. Buranachai, and T. Ha, "Advances in single-molecule fluorescence methods for molecular biology," *Annu. Rev. Biochem.* **77**, 51–76 (2008).
- 20 W. Lee, P. H. von Hippel, and A. H. Marcus, "Internally labeled Cy3/Cy5 DNA constructs show greatly enhanced photo-stability in single-molecule FRET experiments," *Nucleic Acids Res.* **42**, 5967–5977 (2014).
- 21 J. Widengren and P. Schwille, "Characterization of photoinduced isomerization and back-isomerization of the cyanine dye Cy5 by fluorescence correlation spectroscopy," *J. Phys. Chem. A* **104**, 6416–6428 (2000).
- 22 H. Asanuma, T. Fujii, T. Kato, and H. Kashida, "Coherent interactions of dyes assembled on DNA," *J. Photochem. Photobiol. C* **13**, 124–135 (2012).
- 23 P. D. Cunningham, A. Khachatryan, S. Buckhout-White, J. R. Deschamps, E. R. Goldman, I. L. Medintz, and J. S. Melinger, "Resonance energy transfer in DNA duplexes labeled with localized dyes," *J. Phys. Chem. B* **118**, 14555–14565 (2014).
- 24 P. D. Cunningham, Y. C. Kim, S. A. Díaz, S. Buckhout-White, D. Mathur, I. L. Medintz, and J. S. Melinger, "Optical properties of vibronically coupled Cy3 dimers on DNA scaffolds," *J. Phys. Chem. B* **122**, 5020–5029 (2018).
- 25 M. S. Barclay, S. K. Roy, J. S. Huff, O. A. Mass, D. B. Turner, C. K. Wilson, D. L. Kellis, E. A. Terpetschnig, J. Lee, P. H. Davis, B. Yurke, W. B. Knowlton, and R. D. Pensack, "Rotaxane rings promote oblique packing and extended

- lifetimes in DNA-templated molecular dye aggregates,” *Commun. Chem.* **4**, 19 (2021).
- ²⁶S. Hart, W. J. Chen, J. L. Banal, W. P. Bricker, A. Dodin, L. Markova, Y. Vyborna, A. P. Willard, R. Haner, M. Bathe, and G. Schlau-Cohen, “Engineering couplings for exciton transport using synthetic DNA scaffolds,” *Chem* **7**, 827 (2021).
- ²⁷J. D. Hybl, A. W. Albrecht, S. M. Gallagher Faeder, and D. M. Jonas, “Two-dimensional electronic spectroscopy,” *Chem. Phys. Lett.* **297**, 307–313 (1998).
- ²⁸D. M. Jonas, “Two-dimensional femtosecond spectroscopy,” *Annu. Rev. Phys. Chem.* **54**, 425–463 (2003).
- ²⁹P. Hamm and M. T. Zanni, *Concepts and Methods of 2D Infrared Spectroscopy* (Cambridge University Press, 2011).
- ³⁰J. C. Wright, “Analytical chemistry, multidimensional spectral signatures, and the future of coherent multidimensional spectroscopy,” *Chem. Phys. Lett.* **662**, 1–13 (2016).
- ³¹P. J. Sanstead, P. Stevenson, and A. Tokmakoff, “Sequence-dependent mechanism of DNA oligonucleotide dehybridization resolved through infrared spectroscopy,” *J. Am. Chem. Soc.* **138**, 11792–11801 (2016).
- ³²L. Kringle, N. P. D. Sawaya, J. Widom, C. Adams, M. G. Raymer, A. Aspuru-Guzik, and A. H. Marcus, “Temperature-dependent conformations of exciton-coupled Cy3 dimers in double-stranded DNA,” *J. Chem. Phys.* **148**, 085101 (2018).
- ³³D. Heussman, J. Kittell, P. H. von Hippel, and A. H. Marcus, “Temperature-dependent local conformations and conformational distributions of cyanine dimer labeled single-stranded-double-stranded DNA junctions by 2D fluorescence spectroscopy,” *J. Chem. Phys.* **156**, 045101 (2022).
- ³⁴K. L. M. Lewis and J. P. Ogilvie, “Probing photosynthetic energy and charge transfer with two-dimensional electronic spectroscopy,” *J. Phys. Chem. Lett.* **3**, 503–510 (2012).
- ³⁵G. D. Scholes, T. Mirkovic, D. B. Turner, F. Fassioli, and A. Buchleitner, “Solar light harvesting by energy transfer: From ecology to coherence,” *Energy Environ. Sci.* **5**, 9374–9393 (2012).
- ³⁶V. Tiwari, W. K. Peters, and D. M. Jonas, “Electronic resonance with anti-correlated pigment vibrations drives photosynthetic energy transfer outside the adiabatic framework,” *Proc. Natl. Acad. Sci. U. S. A.* **110**, 1203–1208 (2013).
- ³⁷E. Thyryhaug, R. Tempelaar, M. J. P. Alcocer, K. Židek, D. Bina, J. Knoester, T. L. C. Jansen, and D. Zigmantas, “Identification and characterization of diverse coherences in the Fenna–Matthews–Olson complex,” *Nat. Chem.* **10**, 780–786 (2018).
- ³⁸J. Cao, R. J. Cogdell, D. F. Coker, H.-G. Duan, J. Hauer, U. Kleinekathofer, T. L. C. Jansen, T. Mancal, R. J. D. Miller, J. P. Ogilvie, V. I. Prokhorenko, T. Renger, H.-S. Tan, R. Tempelaar, M. Thorwart, E. Thyryhaug, S. Westenhoff, and D. Zigmantas, “Quantum biology revisited,” *Sci. Adv.* **6**, eaaz4888 (2020).
- ³⁹S. Mukamel, *Principles of Nonlinear Optical Spectroscopy* (Oxford University Press, New York, 1995).
- ⁴⁰T. Azumi and K. Matsuzaki, “What does the term ‘vibronic coupling’ mean?,” *Photochem. Photobiol.* **25**, 315–326 (1977).
- ⁴¹B. L. Cannon, D. L. Kellis, L. K. Patten, P. H. Davis, J. Lee, E. Graugnard, B. Yurke, and W. B. Knowlton, “Coherent exciton delocalization in a two-state DNA-templated dye aggregate system,” *J. Phys. Chem. A* **121**, 6905–6916 (2017).
- ⁴²B. L. Cannon, L. K. Patten, D. L. Kellis, P. H. Davis, J. Lee, E. Graugnard, B. Yurke, and W. B. Knowlton, “Large Davydov splitting and strong fluorescence suppression: An investigation of exciton delocalization in DNA-templated Holliday junction dye aggregates,” *J. Phys. Chem. A* **122**, 2086–2095 (2018).
- ⁴³V. T. Ravikumar, T. K. Wyrzykiewicz, and D. L. Cole, “Synthesis of oligonucleotides via phosphoramidite approach utilizing 2-diphenylmethylsilylethyl (DPSE) as a phosphorus protecting group,” *Tetrahedron* **50**, 9255–9266 (1994).
- ⁴⁴A. Meares, K. Susumu, D. Mathur, S. H. Lee, O. A. Mass, J. Lee, R. D. Pensack, B. Yurke, W. B. Knowlton, J. S. Melinger, and I. L. Medintz, “Synthesis of substituted Cy5 phosphoramidite derivatives and their incorporation into oligonucleotides using automated DNA synthesis,” *ACS Omega* **7**, 11002–11016 (2022).
- ⁴⁵J. SantaLucia, “A unified view of polymer, dumbbell, and oligonucleotide DNA nearest-neighbor thermodynamics,” *Proc. Natl. Acad. Sci. U. S. A.* **95**, 1460–1465 (1998).
- ⁴⁶J. R. Lakowicz, *Principles of Fluorescence Spectroscopy*, 3rd ed. (Springer, New York, 2006).
- ⁴⁷L. A. Bizimana, J. Brazard, W. P. Carbery, T. Gellen, and D. B. Turner, “Resolving molecular vibronic structure using high-sensitivity two-dimensional electronic spectroscopy,” *J. Chem. Phys.* **143**, 164203 (2015).
- ⁴⁸B. K. Petkov, T. A. Gellen, C. A. Farfan, W. P. Carbery, B. E. Hetzler, D. Trauner, X. Li, W. J. Glover, D. J. Ulness, and D. B. Turner, “Two-dimensional electronic spectroscopy reveals the spectral dynamics of Förster resonance energy transfer,” *Chem* **5**, 2111 (2019).
- ⁴⁹B. Pinto-Pacheco, W. P. Carbery, S. Khan, D. B. Turner, and D. Buccella, “Fluorescence quenching effects of tetrazines and their Diels–Alder products: Mechanistic insight toward fluorogenic efficiency,” *Angew. Chem., Int. Ed.* **59**, 22140–22149 (2020).
- ⁵⁰M. S. Barclay, J. S. Huff, R. D. Pensack, P. H. Davis, W. B. Knowlton, B. Yurke, J. C. Dean, P. C. Arpin, and D. B. Turner, “Characterizing mode anharmonicity and Huang–Rhys factors using models of femtosecond coherence spectra,” *J. Phys. Chem. Lett.* **13**, 5413–5423 (2022).
- ⁵¹J. R. Taylor, *An Introduction to Error Analysis: The Study of Uncertainties in Physical Measurements*, 2nd ed. (University Science Books, 1997).
- ⁵²R. Trebino, K. W. DeLong, D. N. Fittinghoff, J. N. Sweetser, M. A. Krumbügel, B. A. Richman, and D. J. Kane, “Measuring ultrashort laser pulses in the time-frequency domain using frequency-resolved optical gating,” *Rev. Sci. Instrum.* **68**, 3277–3296 (1997).
- ⁵³U. Selig, F. Langhojer, F. Dimler, T. Löhrlig, C. Schwarz, B. Gieseck, and T. Brixner, “Inherently phase-stable coherent two-dimensional spectroscopy using only conventional optics,” *Opt. Lett.* **33**, 2851–2853 (2008).
- ⁵⁴I. A. Heisler, R. Moca, F. V. A. Camargo, and S. R. Meech, “Two-dimensional electronic spectroscopy based on conventional optics and fast dual chopper data acquisition,” *Rev. Sci. Instrum.* **85**, 063103 (2014).
- ⁵⁵J. Brazard, L. A. Bizimana, and D. B. Turner, “Accurate convergence of transient-absorption spectra using pulsed lasers,” *Rev. Sci. Instrum.* **86**, 053106 (2015).
- ⁵⁶T. A. Gellen, L. A. Bizimana, W. P. Carbery, I. Breen, and D. B. Turner, “Ultrabroadband two-quantum two-dimensional electronic spectroscopy,” *J. Chem. Phys.* **145**, 064201 (2016).
- ⁵⁷D. B. Turner, “Standardized specifications of 2D optical spectrometers,” *Results Chem.* **1**, 100001 (2019).
- ⁵⁸M. Khalil, N. Demirdöven, and A. Tokmakoff, “Obtaining absorptive line shapes in two-dimensional infrared vibrational correlation spectra,” *Phys. Rev. Lett.* **90**, 047401 (2003).
- ⁵⁹J. D. Hybl, A. Albrecht Ferro, and D. M. Jonas, “Two-dimensional Fourier transform electronic spectroscopy,” *J. Chem. Phys.* **115**, 6606–6622 (2001).
- ⁶⁰T. A. Gellen, J. Lem, and D. B. Turner, “Probing homogeneous line broadening in CdSe nanocrystals using multidimensional electronic spectroscopy,” *Nano Lett.* **17**, 2809–2815 (2017).
- ⁶¹M. J. Frisch, G. W. Trucks, H. B. Schlegel, G. E. Scuseria, M. A. Robb, J. R. Cheeseman, G. Scalmani, V. Barone, G. A. Petersson, H. Nakatsuji, X. Li, M. Caricato, A. V. Marenich, J. Bloino, B. G. Janesko, R. Gomperts, B. Mennucci, H. P. Hratchian, J. V. Ortiz, A. F. Izmaylov, J. L. Sonnenberg, D. Williams-Young, F. Ding, F. Lipparini, F. Egidi, J. Goings, B. Peng, A. Petrone, T. Henderson, D. Ranasinghe, V. G. Zakrzewski, J. Gao, N. Rega, G. Zheng, W. Liang, M. Hada, M. Ehara, K. Toyota, R. Fukuda, J. Hasegawa, M. Ishida, T. Nakajima, Y. Honda, O. Kitao, H. Nakai, T. Vreven, K. Throssell, J. A. Montgomery, Jr., J. E. Peralta, F. Ogliaro, M. J. Bearpark, J. J. Heyd, E. N. Brothers, K. N. Kudin, V. N. Staroverov, T. A. Keith, R. Kobayashi, J. Normand, K. Raghavachari, A. P. Rendell, J. C. Burant, S. S. Iyengar, J. Tomasi, M. Cossi, J. M. Millam, M. Klene, C. Adamo, R. Cammi, J. W. Ochterski, R. L. Martin, K. Morokuma, O. Farkas, J. B. Foresman, and D. J. Fox, Gaussian 16 Revision C.01, Gaussian, Inc., Wallingford, CT, 2016.
- ⁶²Y. Zhao and D. G. Truhlar, “The Mo6 suite of density functionals for main group thermochemistry, thermochemical kinetics, noncovalent interactions, excited states, and transition elements: Two new functionals and systematic testing of four Mo6-class functionals and 12 other function,” *Theor. Chem. Acc.* **120**, 215–241 (2008).
- ⁶³J. Tomasi, B. Mennucci, and R. Cammi, “Quantum mechanical continuum solvation models,” *Chem. Rev.* **105**, 2999–3093 (2005).

- ⁶⁴E. Cancès, B. Mennucci, and J. Tomasi, "A new integral equation formalism for the polarizable continuum model: Theoretical background and applications to isotropic and anisotropic dielectrics," *J. Chem. Phys.* **107**, 3032–3041 (1997).
- ⁶⁵D. Van Der Spoel, E. Lindahl, B. Hess, G. Groenhof, A. E. Mark, and H. J. C. Berendsen, "GROMACS: Fast, flexible, and free," *J. Comput. Chem.* **26**, 1701–1718 (2005).
- ⁶⁶M. Zgarbová, J. Šponer, M. Otyepka, T. E. Cheatham III, R. Galindo-Murillo, and P. Jurečka, "Refinement of the sugar–phosphate backbone torsion beta for AMBER force fields improves the description of Z- and B-DNA," *J. Chem. Theory Comput.* **11**, 5723–5736 (2015).
- ⁶⁷R. Galindo-Murillo, J. C. Robertson, M. Zgarbová, J. Šponer, M. Otyepka, P. Jurečka, and T. E. Cheatham, "Assessing the current state of amber force field modifications for DNA," *J. Chem. Theor. Comput.* **12**, 4114–4127 (2016).
- ⁶⁸J. Yoo and A. Aksimentiev, "Improved parametrization of Li⁺, Na⁺, K⁺, and Mg²⁺ ions for all-atom molecular dynamics simulations of nucleic acid systems," *J. Phys. Chem. Lett.* **3**, 45–50 (2012).
- ⁶⁹J. Wang, R. M. Wolf, J. W. Caldwell, P. A. Kollman, and D. A. Case, "Development and testing of a general amber force field," *J. Comput. Chem.* **25**, 1157–1174 (2004).
- ⁷⁰C. I. Bayly, P. Cieplak, W. Cornell, and P. A. Kollman, "A well-behaved electrostatic potential based method using charge restraints for deriving atomic charges: The RESP model," *J. Phys. Chem.* **97**, 10269–10280 (1993).
- ⁷¹E. F. Pettersen, T. D. Goddard, C. C. Huang, E. C. Meng, G. S. Couch, T. I. Croll, J. H. Morris, and T. E. Ferrin, "UCSF ChimeraX: Structure visualization for researchers, educators, and developers," *Protein Sci.* **30**, 70–82 (2021).
- ⁷²W. L. Jorgensen, J. Chandrasekhar, J. D. Madura, R. W. Impey, and M. L. Klein, "Comparison of simple potential functions for simulating liquid water," *J. Chem. Phys.* **79**, 926–935 (1983).
- ⁷³B. Hess, H. Bekker, H. J. C. Berendsen, and J. G. E. M. Fraaije, "LINCS: A linear constraint solver for molecular simulations," *J. Comput. Chem.* **18**, 1463–1472 (1997).
- ⁷⁴G. Bussi, D. Donadio, and M. Parrinello, "Canonical sampling through velocity rescaling," *J. Chem. Phys.* **126**, 014101 (2007).
- ⁷⁵M. Parrinello and A. Rahman, "Polymorphic transitions in single crystals: A new molecular dynamics method," *J. Appl. Phys.* **52**, 7182–7190 (1981).
- ⁷⁶W. West and A. L. Geddes, "The effects of solvents and of solid substrates on the visible molecular absorption spectrum of cyanine dyes," *J. Phys. Chem.* **68**, 837–847 (1964).
- ⁷⁷F. Würthner, S. Yao, T. Debaerdemaeker, and R. Wortmann, "Dimerization of merocyanine dyes. Structural and energetic characterization of dipolar dye aggregates and implications for nonlinear optical materials," *J. Am. Chem. Soc.* **124**, 9431–9447 (2002).
- ⁷⁸A. Yu, C. A. Tolbert, D. A. Farrow, and D. M. Jonas, "Solvatochromism and solvation dynamics of structurally related cyanine dyes," *J. Phys. Chem. A* **106**, 9407–9419 (2002).
- ⁷⁹N. J. Turro, V. Ramamurthy, and J. C. Scaiano, *Modern Molecular Photochemistry of Organic Molecules* (University Science Books, 2010).
- ⁸⁰S. J. Strickler and R. A. Berg, "Relationship between absorption intensity and fluorescence lifetime of molecules," *J. Chem. Phys.* **37**, 814–822 (1962).
- ⁸¹C. C. Jumper, P. C. Arpin, D. B. Turner, S. D. McClure, S. Rafiq, J. C. Dean, J. A. Cina, P. A. Kovac, T. Mirkovic, and G. D. Scholes, "Broadband pump-probe spectroscopy quantifies ultrafast solvation dynamics of proteins and molecules," *J. Phys. Chem. Lett.* **7**, 4722–4731 (2016).
- ⁸²J. Lu, Y. Lee, and J. M. Anna, "Extracting the frequency-dependent dynamic Stokes shift from two-dimensional electronic spectra with prominent vibrational coherences," *J. Phys. Chem. B* **124**, 8857–8867 (2020).
- ⁸³F. Sanda, V. Perlik, C. N. Lincoln, and J. Hauer, "Center line slope analysis in two-dimensional electronic spectroscopy," *J. Phys. Chem. A* **119**, 10893–10909 (2015).
- ⁸⁴S. T. Roberts, J. J. Loparo, and A. Tokmakoff, "Characterization of spectral diffusion from two-dimensional line shapes," *J. Chem. Phys.* **125**, 084502 (2006).
- ⁸⁵R. R. Ernst, G. Bodenhausen, and A. Wokaun, *Principles of Nuclear Magnetic Resonance in One and Two Dimensions* (Clarendon Press, Oxford, 1987).
- ⁸⁶C. B. Murray, D. J. Norris, and M. G. Bawendi, "Synthesis and characterization of nearly monodisperse CdE (E = sulfur, selenium, tellurium) semiconductor nanocrystallites," *J. Am. Chem. Soc.* **115**, 8706–8715 (1993).
- ⁸⁷K. Kwac and M. Cho, "Molecular dynamics simulation study of *n*-methylacetamide in water. II. Two-dimensional infrared pump-probe spectra," *J. Chem. Phys.* **119**, 2256–2263 (2003).
- ⁸⁸A. Nemeth, F. Milota, T. Mančal, V. Lukeš, J. Hauer, H. F. Kauffmann, and J. Sperling, "Vibrational wave packet induced oscillations in two-dimensional electronic spectra. I. Experiments," *J. Chem. Phys.* **132**, 184514 (2010).
- ⁸⁹J. Dostál, "Nonresonant coherent two-dimensional spectroscopy," *Spectrochim. Acta A* **267**, 120441 (2022).
- ⁹⁰M. M. Bishop, J. D. Roscioli, S. Ghosh, J. J. Mueller, N. C. Shepherd, and W. F. Beck, "Vibrationally coherent preparation of the transition state for photoisomerization of the cyanine dye Cy5 in water," *J. Phys. Chem. B* **119**, 6905–6915 (2015).
- ⁹¹B. Champagne, M. Guillaume, and F. Zutterman, "TDDFT investigation of the optical properties of cyanine dyes," *Chem. Phys. Lett.* **425**, 105–109 (2006).
- ⁹²B. Le Guennic and D. Jacquemin, "Taking up the cyanine challenge with quantum tools," *Acc. Chem. Res.* **48**, 530–537 (2015).
- ⁹³A. Biaggne, Y. C. Kim, J. S. Meligner, W. B. Knowlton, B. Yurke, and L. Li, "Molecular dynamics simulations of cyanine dimers attached to DNA Holliday junctions," *RSC Adv.* **12**, 28063 (2022).
- ⁹⁴H. Asanuma, K. Murayama, Y. Kamiya, and H. Kashida, "The DNA duplex as an aqueous one-dimensional soft crystal scaffold for photochemistry," *Bull. Chem. Soc. Jpn.* **91**, 1739–1748 (2018).
- ⁹⁵L. P. DeFlores, R. A. Nicodemus, and A. Tokmakoff, "Two-dimensional Fourier transform spectroscopy in the pump-probe geometry," *Opt. Lett.* **32**, 2966–2968 (2007).